doi: 10.56761/EFRE2022.C3-O-007201

# Nickel-based superalloy, relation between non-linear ultrasound and microstructure changes due to creep damages

*Yutaka Ishii[1,*], Kuniaki Ishihara[1], Toshihiro Ohtani[1], Takayuki Sakakibara[2], Masayuki Kamaya[3], Yutarou Ohta[4], Keiji Kubusiro[4]*

[1]*Shonan institute of technology, Fujisawa, Japan*
[2]*Chuo Spring Co., LTD, Miyosi, Japan*
[3]*INSS, Mikatagun, Japan*
[4]*IHI Coporation, Yokohama, Japan*
[*]*k17024@center.shonan-it.ac.jp*

**Abstract.** Nickel-based superalloy, Inconel 718, has high temperature strength effected by γ″($Ni_3Nb$) phase at approximately 973 K. Inconel 718 is characterized in that the γ″-phase disappearance leading to the creep destruction. In the study, we applied the nonlinear ultrasonic for evaluation the creep damage and the microstructural degradation in γ″ for Inconel 718 plates. The nonlinear ultrasonic holds the potential of becoming the primary means of characterizing creep in metals, because it can probe the change of dislocation structure during the creep. Its sensitivity to microstructural evolutions during the creep is often higher than that of linear properties. We elucidated the relationship between microstructural change and the evolutions of nonlinear acoustic characterizations three-wave-interacting, with electromagnetic acoustic resonance (EMAR) throughout the creep lifetime, nonlinearly was relationship change in dislocation density. X-ray diffraction and EBSD, SEM images supported this view.

**Keywords:** Nonlinear-Ultrasonic, Creep, Inconel 718, EMAR, EBSD, X-ray diffraction, SEM.

## 1. Introduction

Nickel-based Superalloy Inconel® 718 shows high temperature strength dues to γ"($Ni_3Nb$) phase at approximately 973 K. Therefore, it can be applied as heat-resistant alloy for gas-turbine disc materials [1]. Inconel 718 was determined in regard to the γ″-phase disappearance leads to destruction in the creep [2]. In the study, we applied nonlinear ultrasonic of γ″-phase creep damage and microstructural degradation of Inconel 718. We analyzed the relations between the microstructural change and the evolutions of nonlinear acoustic characterizations three-wave-interacting [3, 4] with electromagnetic acoustic resonance (EMAR) regarding the creep lifetime. Non-linear ultrasound method based on that phenomenon; the elastic wave propagated to the object is distorted by the microstructure of the substance. The nonlinear ultrasonic shows the possibility to becoming the primary means of characterizing creep in the metals. To find the relationship between the nonlinearity and the microstructure change XRD (X-ray diffraction) [5], Scanning Electron Microscope (SEM) and Electron Backscattering Diffraction (EBSD) [6, 7] were applied.

## 2. Method

### *2.1. Specimen*

We prepared the creep test plate specimen with Inconel 718. Its dimension was 150 mm long, 18 mm wide and 5 mm thick. Heat treatment was ST (solid solution treatment), 1253 K/h cooling speed AC (air cooling). Aging conditions were at 991K/8h-(56 deg/h)-894K/8h AC and γ″-phase was precipitated. The mechanical properties in Inconel 718 were; the tensile strength 1343 MPa, the elongation 17%. Chemical Compositions are shown in Table 1.

### *2.2. EMAR*

We apply EMAR method, during the creep. EMAR process was in the combination between ultrasound resonance method and contactless transducer EMAT (electro-magnetic acoustic transducer) [4] that were developed for the contactless measurement of phase velocity and attenuation. EMAR method is able to less contact non-linearity measurement.

**Table1.** Chemical Compositions of Inconel 718 (Mass%)

| C | Mn | Si | P | S | Cr | Ni | Mo | Cu | Co |
|---|---|---|---|---|---|---|---|---|---|
| 0.03 | 0.14 | 0.08 | 0.01 | <0.001 | 18.4 | 52.68 | 2.89 | 0.07 | 0.49 |
| **Al** | **Ti** | **Nb** | **Ta** | **Se** | **B** | **Bi** | **Fe** | **Pb** | |
| 0.58 | 0.9 | 5.1 | 0.01 | <0.0003 | 0.004 | <0.0003 | 18.25 | <0.0003 | |

*2.3 Three-wave-interaction method*

We measured with evolutions of the acoustic nonlinearities with the nonlinear three-wave-interaction method throughout the creep life in the gauge section with EMAT. We used bulk-shear-wave EMAT, that transmits and receives shear wave propagating in the thickness direction of a plate type specimen. Three-wave-interaction method is based on the fact that material nonlinearities cause interaction between two intersecting ultrasonic waves. Under certain conditions, this can lead to the generation of third wave with frequency and wave-vector equal to the sum or difference of the incident wave frequencies and wave-vectors, relatively. This is much less sensitive to the system nonlinearities due to spatial selectively, modal selectively, and frequency selectivity. We applied the three-wave-interaction method to EMAR, which was the combination of resonant acoustic technique with EMAT. We measured two EMATs were faced and set in the thickness direction of the sample as shown in Fig.1.

Different resonance frequencies; $f_n$, $f_m$ ($n$, $m$: resonant modes, $m > n$) were generated by two coils, respectively. The difference or sum frequency, $f_n \pm f_m$ was measured by one coil. Because material nonlinearity showed independence of the excitation level, the amplitude of the interaction resonant wave $A_3$, at $f_n \pm f_m$ was normalized to the product of the two input resonant amplitudes $A_1$ and $A_2$. In the study, we measured the amplitude, $A_3$ at the resonant frequency, $f_m - f_n$. In selection of resonance mode, $n$, $m$, the numbers were prime numbers or not with common divisor or common multiple. In the three-wave-interaction method, we used resonant frequency $f_5$ (1.5 MHz) and $f_9$ (2.7 MHz) measured maximum amplitudes, $A_1$, $A_2$ of the different fundamental resonance modes $f_9$–$f_5$ (1.2 MHz) amplitude, and $A_3$ of the incident wave. We measured resonant frequencies for resonant modes with using the systems for a nonlinear acoustic phenomenon (SNAP) manufactured by RITEC (USA).

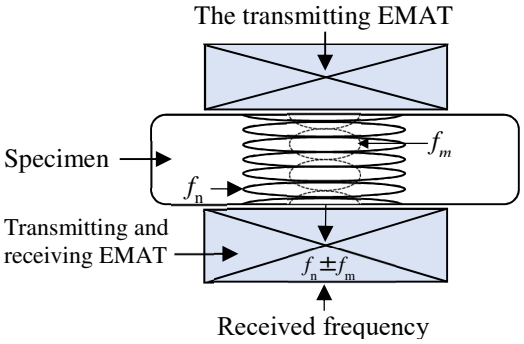


Fig.1. Experimental arrangements for three-wave-interaction, method, Transmitting frequency fa and $f_m$($n$<$m$), Receiver frequency $f_m \pm f_n$.

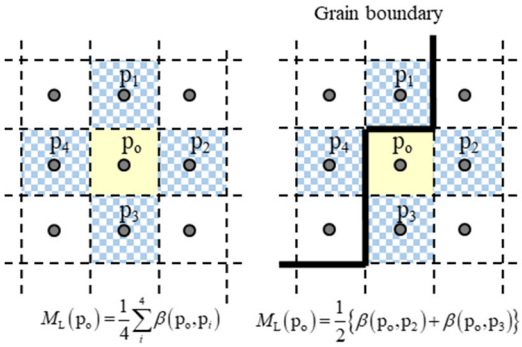


Fig.2. Definition of local misorientation. (ML)

*2.4 Experiments*

To examine the metal structural changes in the creep process of Inconel 718 and the nonlinear ultrasonic characteristics, the creep tests were performed at 973 K and 310 MPa to get the break time of 1810 h. Based on this break, 20%, 40%, 60%, 80%, and 100%of the creep life ratio are created and measured. An experimental setup is presented in Fig.1.

## 3. Microstructural observation

In order to investigate the creep damage process of Inconel 718, we analyzed the crystal misorientation difference with EBSD, the microstructural observation by SEM, and the dislocation density by X-ray diffraction and hardness.

### *3.1 EBSD*

In the crystal misorientation analysis with EBSD method, a small piece of 10×9×5 mm of a cross section of the creep test piece was cut with wire cut for observation EBSD and SEM.

EBSD measurement system (OIM Data Collection ver. 5.2) installed in the field radiation scanning electron microscope (Carl Zeiss ULTRA55), the crystal orientation distribution on the sample surface was measured.

The obtained crystal orientations were measured with Kamaya et al MADAM (Misorientation Analyzer for Damage Measurement) [6, 7] process. The local misorientation, $M_L$, was calculated with the following equation from crystal orientations obtained by the EBSD measurements:

$$M_L(p_0) = \frac{1}{4}\sum_{i=1}^{4}\beta(p_0, p_i), \tag{1}$$

where $\beta(p_0, p_i)$ denotes the misorientation between fixed point $p_0$ and neighboring points $p_i$ in the same grain (Fig.2). A line was drawn between two adjacent points when the misorientation was larger than 5°. If a series of these lines formed a closed region, the lines were defined as grain boundary, and the misorientation between the points of different grains was not included in the calculation of $M_L$.

As the frequency distribution of the local misorientations was well-represented by a log-normal distribution [8], the log-normal average of $M_L$, which is denoted as $M_{ave}$, was calculated for each mapping datum by the following equation [9]:

$$M_{ave} = \exp\left[\frac{1}{n}\sum_{i=1}^{n}\ln\{M_L(p_i)\}\right], \tag{2}$$

where $n$ indicated the number of data. Indicated $n$ is the number of measurement points excluding blank points.

For reference, the parameter *MCD* (Modified Crystal Deformation), defined by the following equation, was calculated from the obtained crystal orientations [8]:

$$MCD = \exp\left[\frac{\sum_{k=1}^{n_g}\{\sum_{i=1}^{n_k}\ln\{\beta(m_k, p_i)\}\}}{\sum_{k=1}^{n_g} n_k}\right], \tag{3}$$

where $\beta(m_k, p_i)$ denotes the misorientation between the central orientation, $m$, of the $k^{th}$ grain and the point $i$ that belongs to the $k^{th}$ grain, and $n_k$ is the number of points included in the grain, $n_g$ is the number of grains. The central orientation was determined as the averaged crystal orientation of all points included in the grain. The frequency distribution of the misorientation from the central orientation was shown to be well-represented by the log-normal distribution for strained and unstrained materials [9]. *MCD* corresponds to the log-normal average of the parameter GROD, which was defined in the commercial software. In addition, since the heading difference contains an error of about 0.1–1°, it is necessary to reduce the influence of error in order to obtain a detailed orientation difference distribution, then the smoothing filter [10] was used.

*3.2 XRD*

In the dislocation density measurement with XRD, Shimad-D1 and M21X were used for the measurement of the half-valent width. The dislocation density was calculated with the Vogt function from a single diffraction profile [5].

## 4. Results and discussion

*4.1 Non-linearity and dislocation*

Fig.3 shows the evolutions of the nonlinearity in three-wave-interaction, $A_3/(A_1A_2)$, ultrasonic attenuation, α. Fig.3a show $A_3/(A_1A_2)$ increases from 60% of the creep life ratio to the rupture. Fig.3b show evolutions of α shows the gradually increase of the 60 % of lifetime; α is increased sharply from 80% until the rupture. Fig.4 shows the relative velocity, $\Delta V/V_0$ and dislocation density $\Lambda_1$ observed with X-ray diffraction during the creep lifetime. Fig.4a show $\Lambda_1$ rise dramatically to 20%, after that, it doesn't change until 80% of lifetime in the creep. $\Lambda_1$ showed rapidly increased from 80 % of lifetime. $\Delta V/V_0$ wasn't change until 80% of lifetime, after that began to decrease until rapture.

This phenomenon shows three-wave-interaction methods nonlinearity $A_3/(A_1A_2)$, attenuation α, dislocation density $\Lambda_1$ as the creep progress was related to the microstructure changes, especially, the dislocation mobility during the creep life.

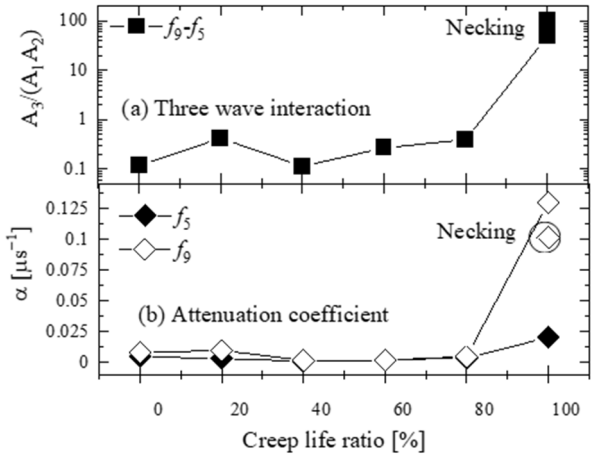


Fig.3. Evolutions of (a) the nonlinearity with three-wave-interaction, (b) attenuation coefficient for Inconel 718 during creep (973 K, 310 MPa, $t_r$ = 1810 h).

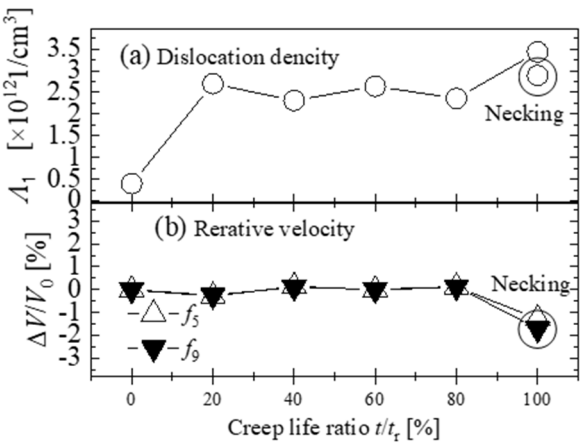


Fig.4. Change of dislocation density (a) and relative velocity (b) for Inconel 718 during creep (973 K, 310 MPa, $t_r$ = 1.810 h).

*4.2* γ″-phase coarsening

The local misorientation $M_L$ with EBSD is shown in Fig.5. An increase in $M_L$ is seen after $t/t_r$ = 60%, the orientation difference is rapidly increased at $t/t_r$ = 100%, and the $M_L$ increases extremely due to the concentration of plastic deformation in the constricted part, and the crystals are miniaturized, as voids are appeared. Inconel 718 precipitated the γ″-phase ($Ni_3Al$) in the mother phase and the functions as a strengthening phase by inhibiting the dislocation motion. $t/t_r$ = 60%, there is an increase in the $M_L$, so it was thought that the function of the strengthening phase was lost due to coarse of γ″-phase.

Fig.6 shows $M_{ave}$ and *MCD* change in the creep life. The parameter showed increase from $t/t_r$ = 60% of the creep life until the rupture. In the $M_{ave}$ and *MCD* indicated increases in dislocation density and microstructural change within grains, and the phenomenon shows to coarse of γ″-phase.

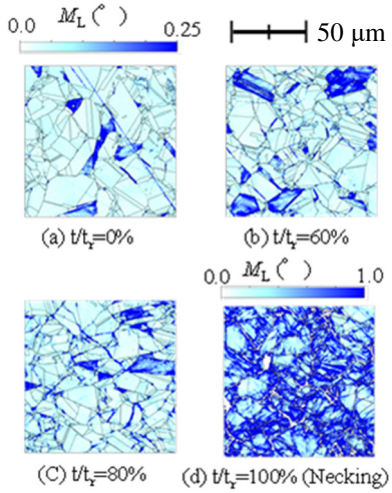


Fig.5. $M_L$ mapping during the creep in Inconel 718 (973 K, 310 MPa, $t_r$ = 1.810 h) [(a) $t/t_r$ = 0%, (b) $t/t_r$ = 60%, (c) $t/t_r$ = 80, (d) $t/t_r$ = 100% (necking area, Max angle 1.0°)].

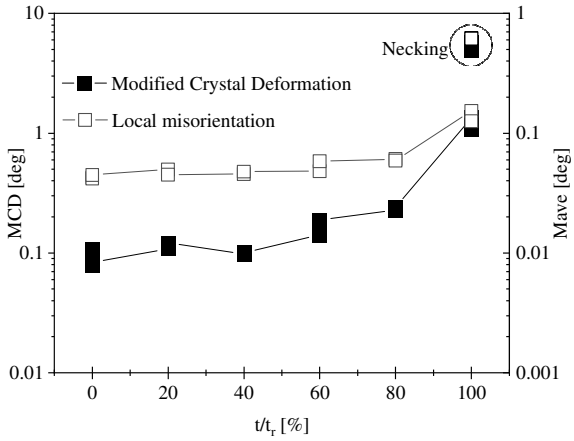


Fig.6. Changes of local misorientation average ($M_{ave}$) and *MCD* during the creep Inconel 718. (973 K, 310 MPa, $t_r$ = 1.810 h).

Fig.7 shows changing γ″ phase image with SEM observation in the creep life. At $t/t_r$ = 0%, it can be seen that MC carbide is precipitated white at the grain boundary. From $t/t_r$ = 60%, a plate like tissue appears in the grain. At $t/t_r$ = 80%, there is a large amount of plate like tissue in the grain. This plate like tissue is considered as to be the γ-phase precipitated from the γ″-phase [2]. γ″-phase and γ-phase both have the same composition as Ni3Nb, however the γ″-phase is body core cubic crystal, and the δ-phase is orthorhombic crystal. This observation indicates that the γ″-phase coarsened and transformed into the δ-phase for creep [11]. These phenomena are indicated the Fig.3a shows $A_3/(A_1A_2)$ behaver was relationship between coarse in γ″-phase with mobile dislocation density increase in the creep.

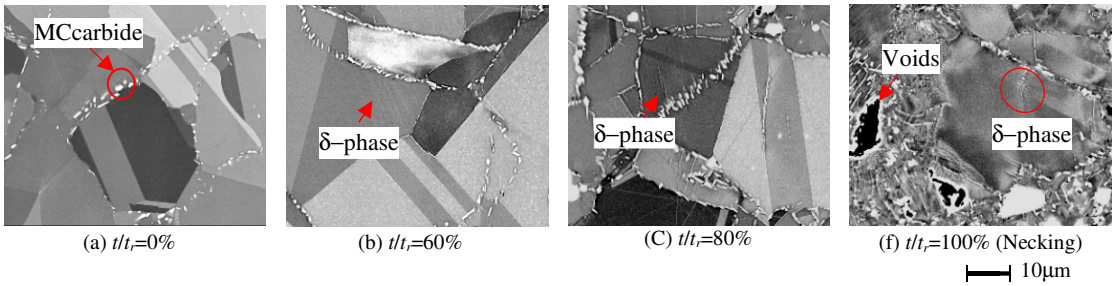


Fig.7. SEM images under creep in Inconel718 (973 K, 310 MPa).

## 5. Conclusion

We investigated the relation between the microstructural change and the evolutions of nonlinear acoustic characterization three-wave-interaction, with EMAR throughout the creep life in Inconel 718. Nonlinear acoustic parameter and ultrasonic attenuation increased from 60% of the creep life, then rapidly increased from 80% of the creep life to the rupture. We interpreted these phenomena in terms of dislocation recovery, recrystallization, and restructuring related to the γ″-phase collapse, with support from the X-ray diffraction, SEM, and EBSD observation.

Nonlinear Elasticity of Solid is caused by lattice anharmonicity [12, 13], Inelasticity due to Dislocation change [14], and crack opening and closure when an acoustic wave impinges on the crack faces [15, 16]. Granato and Lüke's model shows that dislocation was accompanied by phase delay due to the viscous effect due to ultrasonic stress vibrates and absorbs ultrasonic energy, acoustic

inelasticity in caused by dislocation movement in the solid [17]. It is observed the internal friction with ultrasonic attenuation, and wave deformation from γ”-phases transformation.

Nonlinear three-wave-interaction method with EMAR has potential for the creep damage evaluation of Inconel718.

Assessment of the advanced creep damage and the microstructural changes of the metals may potentially facilitate by the nonlinear acoustics measurement with EMAR. In future, we may have any prospect due to Energy Reflection.

## 6. References


[1] Paulonis D.F., Schirra J.J., *Superalloys*, 13, 2001; doi: 10.7449/2001/SUPERALLOYS_2001_13_23

[2] Hayashi K., Kakehi K., *Journal of the Japan Institute of Metals*, **74**(8), 501, 2010; doi: 10.2320/jinstmet.74.501

[3] Hirao M., *JSNDI*, **56**(6), 292, 2007;

[4] Hirao M., Ogi H., *EMATs for science and industry: nondestructive ultrasonic measurements*, (Boston: Kluwar Academic Publishers, 2003).

[5] Ichikawa K., Fujiyama K., Tanaka K., *Proc. JSME M&M Conference*, OS1204, 2009.

[6] Kamaya M., Wilkinson A.J., Titchmarsh J.M., *Nucl. Eng. Des.*, **235**(6), 713, 2005; doi: 10.1016/j.nucengdes.2004.11.006

[7] Kamaya M., Wilkinson A.J., Titchmarsh J.M., *Acta Materialia*, **54**(2), 539, 2006; doi: 10.1016/j.actamat.2005.08.046

[8] Kamaya M., *Material Characterization*, **60**(2), 125, 2009; doi: 10.1016/j.matchar.2008.07.010

[9] Schwarts A.J., Kumar M., Adams B.L., Field D.P. (eds.), *Electron Backscatter Diffraction in Materials Science Second Edition*, (Springer, 2009).

[10] Kamaya M., *Materials Transactions*, **51**(9), 1516, 2010; doi: 10.2320/matertrans.MAW201005

[11] Weertman J., Weertman J.S., *Elementary dislocation theory*. (Oxford: University Press, 1992).

[12] Wallace D.C., *Thermodynamics of crystals.* (Dover: Publisher, 1972).

[13] Kim K.Y., *Physical Review B*, **54**(9), 6245, 1996; doi: 10.1103/PhysRevB.54.6245

[14] Guyer R.A., McCall K.R., Van Den Abeele K.E.-A., *Geophysical Research Letter*, **25**(10), 1585,1998; doi: 10.1029/98GL51231

[15] Croxford A.J., Wilcox P.D., Drinkwater B.W., Nagy P.B., *JASA*, **126**(5), EL117, 2009; doi: 10.1121/1.3231451

[16] Moises L., Henry B., Richard S., *Handbook of elastic properties of solids, liquids, and gasses. Vol.3*, (Academic Press, 1991).

[17] Granato A., Lücke K., *J. Appl. Phys*., **27**, 583, 1956; doi: 10.1063/1.1722436